Determination of the transient electron temperature in a femtosecond-laser-induced air plasma filament

Zhanliang Sun, Jinhai Chen, and Wolfgang Rudolph

Phys. Rev. E **83**, 046408 — Published 25 April 2011

DOI: 10.1103/PhysRevE.83.046408

Determination of the Transient Electron Temperature in a Femtosecond Laser Induced Air Plasma Filament

Zhanliang Sun,* Jinhai Chen, and Wolfgang Rudolph
University of New Mexico, Department of Physics and Astronomy, Albuquerque, NM, 87131
(Dated: March 9, 2011)

The transient electron temperature in a weakly ionized femtosecond laser produced air plasma filament was determined from optical absorption and diffraction experiments. The electron temperature and plasma density decay on similar time scales of a few hundred picoseconds. Comparison with plasma theory reveals the importance of inelastic collisions that lead to energy transfer to vibrational degrees of freedom of air molecules during the plasma cooling.

PACS numbers: 52.38.Hb, 52.70.Kz , 52.25.-b

* jimsun@unm.edu

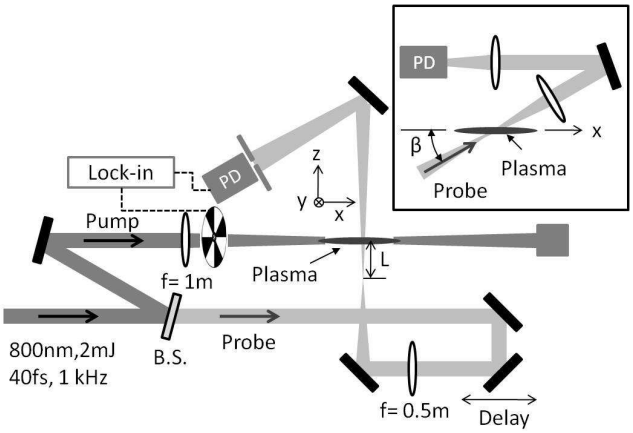

FIG. 1. Experimental setup to probe the transient diffraction and absorption of a fs pulse produced air plasma. The inset shows the diagram for the absorption measurements.

I. INTRODUCTION

Femtosecond pulse induced filaments have gained a great deal of interest in the past two decades (see Refs. [1–3] for recent reviews). Applications range from lightning control and triggering of discharges [4], to remote sensing [5], to few-cycle pulse generation [6, 7]. Filaments are initiated when laser pulses self-focus to intensities large enough to produce multi-photon ionization. The resulting plasma produces a radial refractive index variation (negative lens) counteracting the self-focusing, which leads to filamentation over distances that can exceed several tens of meters depending on the energy and duration of the optical pulse [8] . To take full advantage of the potential these plasma channels offer for many applications their properties including the transient behavior must be known. Two key parameters of laser plasmas are the electron density N_e and electron temperature T_e. Plasma densities produced by filaments in air are on the order of $10^{18}\mathrm{m}^{-3}$ to $10^{24}\mathrm{m}^{-3}$ [9–11]. Previous measurements obtained the electron density from the electric conductivity of the plasma [9, 12], from interferometry measuring the optical phase shift introduced by a plasma channel [10], and by optically probing the plasma induced diffraction [11, 13–15].

More recently, a spectroscopic approach was applied to characterize fs laser filaments in argon gas [16] and air [17]. The plasma density was derived from the Stark broadened fluorescence line width, while the electron temperature was determined from relative line strengths. Typically these techniques average over several nanoseconds (the shorter of the detector integration time and the fluorescence lifetime). Simulations of kinetic processes in air plasmas suggest substantial changes of the electron temperature and electron density on time scales of a few hundred picoseconds [18]. While the transient behavior of the electron density in air plasmas was measured with a fs probe in Ref. [13] the transient electron temperature has not yet been determined with sub ns temporal resolution.

In this paper we determine the transient electron temperature and electron density in an air plasma with ps resolution by measuring the real and imaginary parts of the time dependent refractive index and applying the Drude model. The experimental results are compared to plasma kinetic theory that takes into account elastic and inelastic collisions with ionic and neutral molecules.

II. TRANSIENT ABSORPTION AND DIFFRACTION

A schematic diagram of the experimental setup is shown in Fig. 1. An air plasma channel was produced by focusing the pulses from a 40-fs, 1-kHz, 2-mJ Ti:sapphire oscillator-amplifier system using an $f = 1$ m lens. The beam profile was Gaussian with a beam radius of about 8 mm. The transient absorption and diffraction of the plasma were measured by a time delayed, weak probe pulse.

A pump-probe technique similar to that described in Ref. [13] was applied to measure the transient diffraction. For higher sensitivity and to employ lock-in detection we replaced the CCD camera with a pinhole and photodiode to monitor the negative lens (real part of the dielectric constant) produced by the plasma. The plasma diameter was estimated from the plasma emission to be $d \approx 200$ μm [full width at half maximum (FWHM)]. As will be explained below the probe beam diameter at the position of the plasma was $2d$. L is the distance from the probe's beam waist to the plasma. In addition, we avoided delays at which index changes due to molecular alignment revival are expected [19]. Since our probe diameter was about 0.4 mm each data point represents an average over about 2 ps,

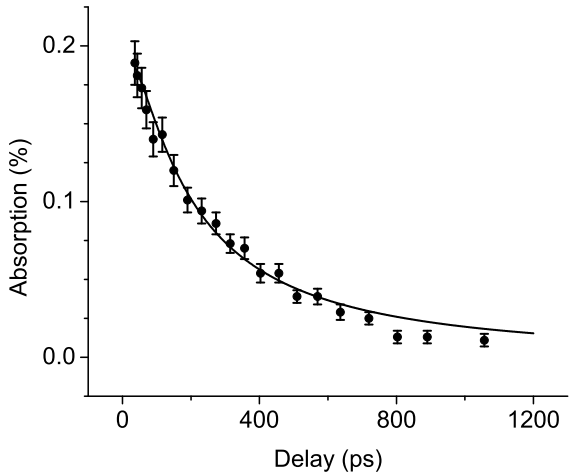

FIG. 2. Measured plasma absorption as a function of the delay (data points). The solid line is a modeling result with an initial Gaussian N_e and initial flat-top T_e profile (see section IV). The error bars represent the combined contribution from the absorption and input power measurements (relative error of the latter $\sim 1\%$).

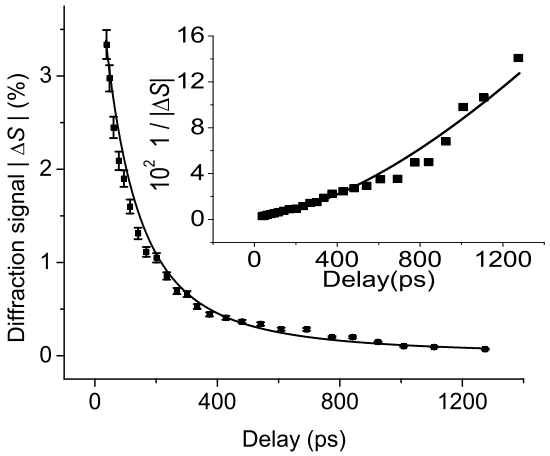

FIG. 3. Measured diffraction signal $|\Delta S|$ as a function of the delay after subtracting an offset of about 0.3% produced by heating of the gas (data points). The solid line is a modeling result with an initial Gaussian N_e and initial flat-top T_e profile (see section IV). The inset shows $1/|\Delta S(t)|$ (data points), which is clearly nonlinear, together with the modeling results (see section IV). The error bars represent the combined contribution from the diffraction and input power measurements and from the far-field approximation.

further reducing the effect of molecular rotation.

For the measurement of the absorption (imaginary part of the dielectric constant), the probe beam was focused through the plasma center ($L = 0$) and the transmitted beam was fully collected by the photodiode with the pinhole removed. To increase the interaction length with the plasma, probe and pump included an angle of $\beta = 30$ degrees (see inset of Fig. 1). The measured absorption (in percent) as a function of delay is depicted in Fig. 2. All results are plotted for delays $\tau > 35$ ps to avoid complications in the data interpretation resulting from pulse overlap and non-equilibrium electron distributions.

Figure 3 shows the measured diffraction signal $|\Delta S|$ as a function of delay. The signal recovers on a time scale of a few hundred ps, similar to what was observed previously [13, 15]. It is interesting to note that the signal recovery is not complete after 1.3 ns and that there is a small signal ($\sim 0.3\%$) even for negative delays (note that ps negative delays actually correspond to a delay of one ms relative to the previous excitation pulse). We attribute this signal,

which decays on a time scale of a few ms, to a temperature increase of the air. The thermal time constant for heat dissipation can be estimated with $\tau_T = \rho_{air} c_p d/(4h) \approx 3$ ms [20], where $\rho_{air} \approx 1$ kg/m^3 is the air density (at 1600 m above sea level), $c_p \approx 1 \times 10^3$ J/(kg K) is the mass specific heat capacity, and $h \approx 15$ W/(m^{2}K) is the heat transfer coefficient. This signal disappeared at repetition rate of 333 Hz.

To relate the diffraction results to the refractive index change we modeled the signal using Fraunhofer diffraction. The distance from the plasma to the detector was at a finite distance of about 1 m. To assess the accuracy of the far-field results, we performed a numerical analysis based on Fresnel diffraction. The results are within 1.5% of those obtained using the far-field approximation. We show here the semi-analytic expression for the Fraunhofer case because they show explicitly the parameter dependencies.

The diffraction geometry and the coordinate system used are shown in Fig. 1, with z (x) being the propagation direction of the probe (pump) and y being perpendicular to both the filament and probe beam axes. The pinhole in front of the detector selects the zero spatial frequency ($\rho = 0$) component of the product of the probe field, $E(x, y)$ and the complex transmission function of the filament, $\exp[i\phi(x, y)]$:

$$\begin{aligned} S(\rho = 0) = S_0 &= |\text{F.T.}\{E(y)\exp[i\phi(y)]\}|^2 \\ &= \frac{C}{w^2}\left|\int \exp\left[-\frac{y^2}{w^2} + ik\left(\frac{y^2}{2R} + \int \tilde{n}(y,z)\mathrm{d}z\right)\right]\mathrm{d}y\right|^2. \end{aligned} \tag{1}$$

Here w and R are the beam radius and the radius of the wavefront of the probe, respectively, at the position of the filament, C is a constant, $k = 2\pi/\lambda$ is the wave vector, and $\tilde{n}$ is the (complex) refractive index. Because of the larger transverse density gradient, the plasma causes diffraction with respect to "y" only. The beam change with respect to the "x" coordinate is that of an undisturbed Gaussian probe beam. For weakly ionized plasmas, as is the case here, the plasma induced index change at $y = z = 0$ is $|\Delta\tilde{n}_m| \ll 1$. From the Drude model it can be shown that the imaginary part of the index n_I is much smaller than the real part Δn_m for electron densities $N_e < 10^{24}$ m^{-3} and its contribution to the diffraction signal can be neglected.

Under these conditions the relative signal change is proportional to the index change

$$\Delta S(L, w_0) = \frac{S_0(\Delta n_m) - S_0(\Delta n_m = 0)}{S_0(\Delta n_m = 0)} \approx Q(L, w_0)\Delta n_m, \tag{2}$$

where the calibration factor Q depends on the waist w_0 of the probe beam, the distance L between the probe waist and the plasma center, and on $\Delta n(y, z)$. The latter is controlled by the electron density distribution. For example, for flat-top and Gaussian transverse electron density profiles of FWHM d =200 μm, $Q \approx 910$ and $Q \approx 520$, respectively, for our experimental geometry ($w_0 = 54$ μm, $L = 20$ mm and a beam M^2 value of 2.1). For Gaussian profiles and $|\Delta n_m| \ll 1$,

$$\begin{aligned} S_0(\Delta n_m) \approx \frac{C}{w^2}\Bigg|&\int \exp\left(-\frac{y^2}{w^2} + \frac{iky^2}{2R}\right)\mathrm{d}y \\ &+ \frac{ikd}{2}\sqrt{\frac{\pi}{\ln 2}}\Delta n_m \int \exp\left(-\frac{y^2}{w^2} - \frac{4\ln 2\, y^2}{d^2} + \frac{iky^2}{2R}\right)\mathrm{d}y\Bigg|^2, \end{aligned} \tag{3}$$

where $w^2 = w_0^2\left[1 + \left(L\lambda M^2/\pi w_0^2\right)^2\right]$. Inserting Eq. (3) into Eq. (2) and neglecting the much smaller Δn_m^2 term, we obtain for Q

$$Q \approx \frac{2\Re\left(\tilde{A}\tilde{B}^*\right)}{\left|\tilde{A}\right|^2}, \tag{4}$$

where $\tilde{A} = \sqrt{\pi/\left(1/w^2 - i\ k/(2R)\right)}$ and $\tilde{B} = i\ (\pi/\sqrt{2\ln 2})kd/\sqrt{2/w^2 - i\ k/R + 8\ln 2/d^2}$.

Because the excitation beam is Gaussian and the plasma is weakly ionized, it is reasonable to assume that the initial electron density can be approximated by a Gaussian profile. Because of the density dependent recombination, the electron density at later times will approach a flat-top profile. For a rough estimation the scale factor Q can be used to obtain the time dependent refractive index changes $\Delta n_m(t)$ and the electron density N_e from the diffraction signal assuming constant (flat-top) profiles as will be explained in the next section.

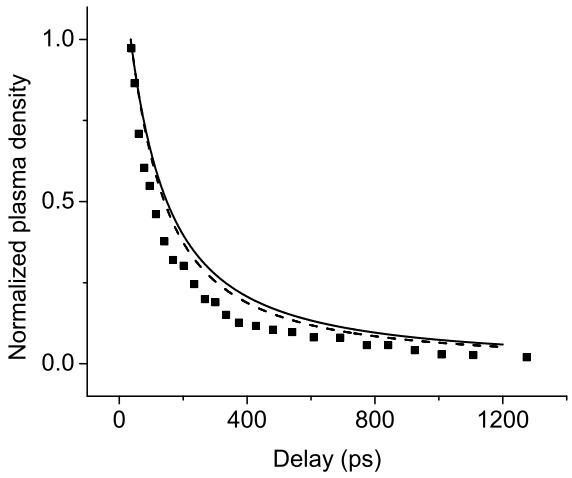

FIG. 4. Plasma density $N_e(r=0)$ as a function of delay. The data points are obtained from the diffraction experiment (data points in Fig. 3) assuming time-invariant flat-top electron density radial distributions. The solid and dashed line are from the model (see section IV) and represent initially flat-top and Gaussian $T_e(r)$ distributions, respectively. The initial electron distribution was Gaussian. The two curves are almost identical.

III. DETERMINATION OF THE INITIAL PLASMA DENSITY AND ELECTRON TEMPERATURE

According to the Drude model of a plasma (see for example [21]), the dielectric constant can be written as

$$\epsilon = 1 - \frac{\omega_{pe}^2}{\omega^2 + i\omega\nu_e} = \tilde{n}^2 = (n + in_I)^2, \tag{5}$$

where ω is the probe laser frequency and $\omega_{pe} = \sqrt{N_e e^2/\epsilon_0 m_e}$ is the plasma frequency. Here e and m_e are the electron charge and mass, respectively, ϵ_0 is the permittivity of free space, and ν_e is the electron collision rate. If we introduce the critical electron density $N_{cr} = \omega^2 m_e \epsilon_0/e^2 \approx 1.74 \times 10^{27}$ m^{-3} for which $\omega_{pe} = \omega$, and use the fact that $\nu_e \ll \omega$ and $N_e \ll N_{cr}$ in an underdense plasma, we can approximate the real part of the refractive index by $n \approx 1 - N_e/(2N_{cr})$. This yields for the plasma induced (real) index change as a function of the plasma density

$$\Delta n(t) \approx -\frac{1}{2}\frac{N_e(t)}{N_{cr}}. \tag{6}$$

If we make the approximation that the shape of the electron density profile does not change in time we can estimate $N_e(r=0)$ at different delays using Eqs. (2) and (6) and the data points from Fig. 3 for flat-top and Gaussian profiles. The data points in Fig. 4 show the normalized electron density assuming a flat-top profile for N_e. The initial plasma density is about $N_{e0} = 1.3 \times 10^{23}$ m^{-3} and $N_{e0} = 2.3 \times 10^{23}$ m^{-3} for flat-top and Gaussian density profiles with FWHM widths $d = 200$ μm, respectively.

The absorption coefficient is proportional to the imaginary part of the refractive index change, $\alpha = 2\omega n_I/c$. Using Eqs.(5) and (6) and the previous approximations it can be written as

$$\alpha(t) \approx \frac{\nu_e(t) N_e(t)}{c N_{cr}}, \tag{7}$$

where c is the speed of light. For $\alpha \ll 1$, the relative absorption change experienced by the probe is

$$A(t) = \frac{E_0 - E_1}{E_0} = \int \alpha(t,z)\mathrm{d}z, \tag{8}$$

where E_0 and E_1 are the input and output probe pulse energies, respectively. To extract the electron temperature we need to evaluate the electron collision rate ν_e contained in Eq. (7). The collision rate can be written as the sum

of the electron - ion and the electron - neutral collision rates $\nu_e = \nu_{ei} + \nu_{en}$ [18]. The electron - ion collision rate in weakly ionized plasmas is given by

$$\nu_{ei}(t) = c_{ei} \ln\Lambda(t) \frac{N_e(t)}{T_e^{3/2}(t)}, \tag{9}$$

where $c_{ei} = e^4/\left(6\epsilon_0{}^2\sqrt{2\pi^3 m_e {k_B}^3}\right)$, k_B is the Boltzmann constant and $\ln\Lambda$ is the Coulomb logarithm [21]. The Coulomb logarithm is weakly dependent on N_e and T_e and is typically used as a constant on the order of 10. The uncertainty of its value increases as $1/|\ln\Lambda|$ [22]. We determined $\ln\Lambda$ from a fit to the experimental data (see next section) and use here $\ln\Lambda \approx 4$.

The electron - neutral collision rate can be expressed as [18]

$$\nu_{en}(t) = N_n \sigma_{en} (k_B/m_e)^{1/2} T_e^{1/2}(t), \tag{10}$$

where $N_n \approx 2.0 \times 10^{25}$ m^{-3} is the density of neutral particles, which can be regarded as time independent in a weakly ionized plasma, and $\sigma_{en} \approx 1 \times 10^{-19}$ m^2 is the collision cross section [18].

Using Eqs. (7) to (10), the measured absorption A, and the initial N_e, we can estimate the initial electron temperature. Assuming a flat-top temperature profile we obtain $T_{e0} \approx 3900$ K for Gaussian $N_{e0}(r)$ while for Gaussian $T_{e0}(r)$ and $N_{e0}(r)$ profiles $T_{e0}(0) \approx 5400$ K. The uncertainty of the initial temperature range is about 8%. In the next section we will apply a kinetic plasma model taking into account the spatial evolution of the electron density and temperature profiles during relaxation to extract $T_e(t)$ from the measurements. The model will also allow us to discuss the evolution of $T_e(r,t)$ and $N_e(r,t)$ transverse profiles.

IV. MODELING AND DISCUSSION

Even though the ionization potential of O_2 is considerably lower than that of N_2 (12.1 eV versus 15.6 eV [21]), for typical pulse intensities in filaments, there can be a non-negligible density of nitrogen ions [23, 24]. During our time scale of interest, the plasma density changes due to the recombination of electrons with ions and the electron and ambient gas temperature change due to elastic and inelastic collisions. The rate equation for the electron density can be written as

$$\frac{\mathrm{d}}{\mathrm{d}t} N_e(t) = -k_{ei} N_e^2(t). \tag{11}$$

With the assumption that k_{ei} is constant a solution to Eq. (11) is $N_e(t) = N_{e0}/(1 + k_{ei} N_{e0} t)$. This expression was previously used to deduce $k_{ei} \approx 1.2 \times 10^{-13}$m^3/s from time-resolved diffraction measurements [13]. For a more accurate description of the recombination process the T_e dependence of the recombination rate must be taken into account, which causes k_{ei} to be a function of time. For a temperature range from 80 K to 11000 K a rate constant of $k_{ei}(T_e) \approx K_0/\sqrt{T_e[\mathrm{K}]}$ m^3/s was deduced from measurements of the electron recombination with both O_2^+ and N_2^+ [25]. The coefficients $K_0(O_2^+) \approx 3.3 \times 10^{-12}$ and $K_0(N_2^+) \approx 6.1 \times 10^{-12}$ are similar but not identical. We will consider in our model the electron temperature dependence of k_{ei} and use K_0 as a fit parameter, which contains the information on the average relative density of singly ionized nitrogen and oxygen molecules.

A constant temperature of $T_e = 1500$ K was used in the expressions for k_{ei} for O_2^+ and N_2^+ to fit $N_e(t)$ data from diffraction experiments in [15]. This temperature can be considered as an average temperature within one ns after excitation.

The relaxation of the electron temperature is controlled by elastic and inelastic collisions between electrons and ionic and neutral molecules:

$$\frac{\mathrm{d}}{\mathrm{d}t} T_e(t) = \frac{2m_e}{m_{i,n}} (\nu_{ei} + \nu_{en})(T_{i,n} - T_e) + V(T_e). \tag{12}$$

Here $m_{i,n}$ ($T_{i,n}$) is the mass (temperature) of the ionized and neutral molecules, which are assumed to be equal, and we also do not distinguish here between oxygen and nitrogen. The introduced errors are small. The first summand describes the energy transfer due to elastic collisions according to the Landau-Spitzer model [21]. The second term takes into account inelastic collisions exciting molecular vibrational degrees of freedom.

The energy transfer rate to vibrational degrees of freedom of O_2 and N_2 molecules can be written as

$$\frac{3k_B}{2} V(T_e) = -\frac{(T_e - T_b)}{T_e} \sqrt{\frac{k_B T_e}{m_e}} N_n \left[0.79\sigma_{N_2}(T_e)\epsilon_{N_2} + 0.21\sigma_{O_2}(T_e)\epsilon_{O_2}\right], \tag{13}$$

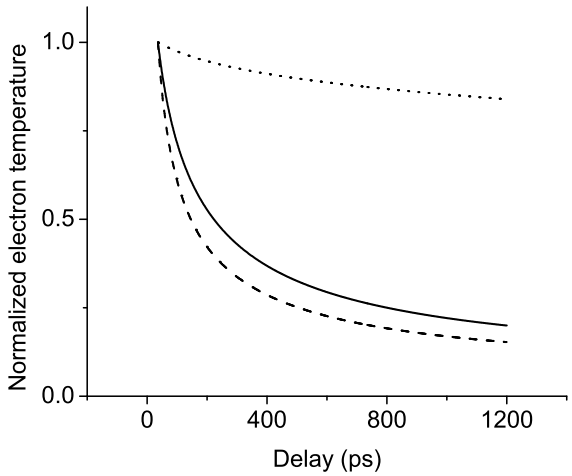

FIG. 5. Normalized electron temperature $T_e(r=0)$ as a function of delay. The solid and dashed line are from a fit of the model to the experimental data and represent initially flat-top and Gaussian $T_e(r)$ distributions, respectively. The initial electron distribution was Gaussian. The dotted line was calculated with the same parameters as the solid line but without inelastic collisions.

where σ_x is the inelastic collisional cross section for collisions with nitrogen and oxygen molecules and $\epsilon_{N_2(O_2)} = 0.29$ eV (0.20 eV) is the vibrational energy quantum of N_2 (O_2) [21]. The experimentally obtained inelastic collision cross sections can be approximated analytically by

$$\sigma_{N_2(O_2)} = a_0^2 \exp\left[\sum_{k=0}^{4} b_k \ln\left(\frac{T_e k_B}{e}\right)^k\right], \tag{14}$$

where $a_0^2 = 2.8 \times 10^{-21}$ m^2, $b_0 = 2.172$, $b_1 = 1.799$, $b_2 = -0.6725$, $b_3 = 0.0954$, $b_4 = -0.00565$ for N_2, and $b_0 = 2.465$, $b_1 = 0.825$, $b_2 = -0.2325$, $b_3 = 0.0194$ and $b_4 = -0.00094$ for O_2 [26].

We assume that the temperature of ions and neutral molecules (background temperature) is equal with an initial value of 300 K. This background temperature changes according to

$$\frac{\mathrm{d}}{\mathrm{d}t}T_b(t) = -\frac{3k_B N_e}{\rho c_p}\frac{\mathrm{d}T_e}{\mathrm{d}t}\bigg|_{elastic}. \tag{15}$$

During our time scale of interest, only elastic collisions lead to an increase in the molecules kinetic energy (temperature). The vibrational degrees of freedom excited through inelastic collisions exchange energy with translational degrees of freedom (VT relaxation) slowly and the corresponding time constants are much greater than a few ms [27, 28].

The rate equations (11), (12) and (15) are solved numerically. We take into account the radial (r) dependence of the temperature and electron density and compute the diffraction and absorption. We assume that initially the electron density $N_e(r)$ is Gaussian and use the corresponding initial value of 2.3×10^{23} m^{-3}. The initial electron temperature is controlled by the kinetic energy of the electrons after multi-photon ionization of O_2 and N_2. It should be noted that inverse bremsstrahlung has only a minor effect on the electron energy for sub 100 fs pulses. In the limit where multi-photon absorption dominates, the photon energy rather than the intensity profile $I(r)$ controls the initial $T_e(r)$, which is then best described by a flat-top profile. Although for our laser and beam parameters tunneling ionization cannot be neglected we will assume this initial temperature profile with the previously estimated $T_{e0} = 3900$ K. To evaluate the impact of this assumption we will compare the results to an initially Gaussian temperature profile later.

Free parameters are the Coulomb logarithm and K_0, which are determined from a simultaneous best fit to the diffraction and absorption measurements. For $\ln\Lambda = 4$ and $K_0 = 2.1 \times 10^{-12}$, the modeling results and the measurements are shown in Figs. 2 and 3 showing good agreement overall. For comparison we also evaluated the case of an initially Gaussian temperature profile $T_e(r)$ with a peak value of $T_{e0} = 5400$ K. The relaxation of N_e and T_e at the center of the plasma is depicted in Figs. 4 and 5. It is obvious that the decay curve $N_e(t)$ is less sensitive to the assumed initial radial distributions of the plasma parameters than $T_e(t)$.

The electron temperature averaged over 1 ns for an initially flat-top T_e profile is in good agreement with the 1500 K used in [15] to define a temperature independent rate k_{ei}. It should also be mentioned that if we use separate

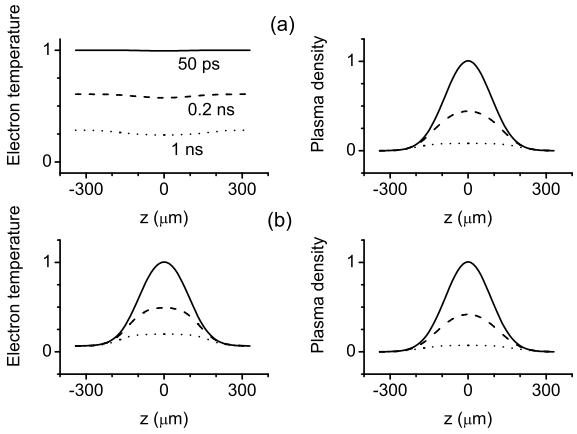

FIG. 6. Calculated electron temperature and density profiles at different delay times for two sets of initial profiles ($x = y = 0$). (a) flat-top $T_{e0}(r)$, Gaussian $N_{e0}(r)$, (b) Gaussian $T_{e0}(r)$ and $N_{e0}(r)$.

recombination equations for O_2^+ and N_2^+ with the published k_{ei} coefficients [25], the initial ion ratio becomes a free parameter. With $N_{O2+}/N_{N2+} \approx 3.3$ we obtain a similarly good agreement with the experimental results. This ion ratio is what one can expect for our experimental conditions using the ionization rates from [24].

The inelastic collisions exciting molecular vibrations play a major role in the relaxation of the electron temperature as can be seen in Fig. 5. In plasmas produced in atomic gases, there are no vibrational degrees of freedom and consequently the corresponding rate $V(T_e) = 0$. This can explain the relatively high average electron temperature observed in a fs pulse produced argon plasma of $T_e \approx 5500$ K [16]. Since the measurement was based on relative emission line strengths from a Boltzmann plot the reported temperature was an average over about 10 ns (integration time of camera).

Figure 6 shows the normalized radial distributions of T_e and N_e at three different time delays for initially Gaussian and flat-top $T_e(r)$ with Gaussian $N_e(r)$ profiles. The electron temperature at the plasma center relaxes faster compared to the outer regions. This is a result of the dependence of the elastic collision term in Eq. (12) on the electron density through ν_{ei}. The electron density flattens because of the bimolecular nature of the recombination process.

The start point of the simulations refers to the experimental data at a delay of 35 ps. If we extrapolate the initial values to zero delay the electron temperature would be about 20% higher and the electron density about 50% times larger than the values mentioned before.

Since the experiments were carried out with a 1-kHz pulse train the average ambient temperature of the volume immediately surrounding the plasma is higher than room temperature (300 K). A simple heat diffusion model estimates a temperature increase of a few ten degrees with a FWHM of the distribution of $D \approx 1$ mm. Changing the ambient temperature by 50 K does not affect the previously derived results noticeably. The aforementioned 0.3% diffraction signal at negative delays is a result of this temperature increase and the heat deposition by the preceding single pulse in a cylinder of diameter d.

The classical description of the dielectric constant by the Drude model using effective collision rates is an approximation. The electron - electron collision rate [26] at the center of the plasma is between 3.3×10^{13} Hz and 5.5×10^{13} Hz for delay times between 35 ps and 1200 ps. The sum of the rates for ion - ion and ion - neutral collisions [29] is between 6×10^{11} Hz and 1.0×10^{13} Hz in the same delay range. The corresponding time scales to reach equilibrium are therefore less than 10 ps. The model assumes electrons and ions with well defined energies rather than distribution functions. The electron and ion densities therefore must be considered as averages.

V. SUMMARY

A time-resolved optical method and a kinetic plasma model were developed to determine the transient electron density N_e and the temperature T_e distribution in a fs pulse produced air plasma. The electron temperature decays on a time scale of a few hundred ps. Initial electron temperatures of 3900 K were obtained for initially flat-top temperature and Gaussian electron transverse density distributions with initial peak values of 2.3×10^{23} m^{-3}. The experimental results were modeled with plasma kinetic theory taking into account elastic and inelastic collisions

between electrons, ions, and neutral molecules, including their vibrational degrees of freedom as well as the radial dependence of electron temperature and density. The results indicate the importance of molecular vibrational degrees of freedom in the cooling of the electron gas. While the initial values for N_e and T_e depend on the assumed initial transverse profiles the decay transients are rather independent.

ACKNOWLEDGMENTS

We are grateful to Z. Wang, L. A. Emmert, C. Rodriguez, D. Cremers, and R. Multari for helpful discussions and support with the experiments. This work was supported by NSF (PHY-0722622) and ONR (N000140810350).

[1] L. Bergé, S. Skupin, R. Nuter, J. Kasparian, and J.-P. Wolf, Rep. Prog. Phys. **70**, 1633 (2007).
[2] A. Couairon and A. Mysyrowicz, Phys. Rep. **441**, 47 (2007).
[3] V. P. Kandidov, S. A. Shlenov, and O. G. Kosareva, Quantum Electron. **39**, 205 (2009).
[4] X. M. Zhao, J.-C. Diels, C. Y. Wang, and J. M. Elizondo, IEEE J. Quantum Electron. **31**, 599 (1995).
[5] J. Kasparian, M. Rodriguez, G. Méjean, J. Yu, E. Salmon, H. Wille, R. Bourayou, S. Frey, Y.-B. André, A. Mysyrowicz, R. Sauerbrey, J.-P. Wolf, and L. Wöste, Science **301**, 61 (2003).
[6] N. L. Wagner, E. A. Gibson, T. Popmintchev, I. P. Christov, M. M. Murnane, and H. C. Kapteyn, Phys. Rev. Lett. **93**, 173902 (2004).
[7] A. Couairon, J. Biegert, C. P. Hauri, W. Kornelis, F. W. Helbing, U. Keller, and A. Mysyrowicz, J. Mod. Opt. **53**, 75 (2006).
[8] A. Braun, G. Korn, X. Liu, D. Du, J. Squier, and G. Mourou, Opt. Lett. **20**, 73 (1995).
[9] H. Schillinger and R. Sauerbrey, Appl. Phys. B: Lasers Opt. **68**, 753 (1999).
[10] H. Yang, J. Zhang, Y. Li, J. Zhang, Y. Li, Z. Chen, H. Teng, Z. Wei, and Z. Sheng, Phys. Rev. E **66**, 016406 (2002).
[11] F. Théberge, W. Liu, P. T. Simard, A. Becker, and S. L. Chin, Phys. Rev. E **74**, 036406 (2006).
[12] A. Ting, I. Alexeev, D. Gordon, R. Fischer, D. Kaganovich, T. Jones, E. Briscoe, J. Peñano, R. Hubbard, and P. Sprangle, Phys. Plasmas **12**, 056705 (2005).
[13] S. Tzortzakis, B. Prade, M. Franco, and A. Mysyrowicz, Opt. Commun. **181**, 123 (Jul. 2000).
[14] J. Liu, Z. Duan, Z. Zeng, X. Xie, Y. Deng, R. Li, Z. Xu, and S. L. Chin, Phys. Rev. E **72**, 026412 (2005).
[15] G. Rodriguez, A. R. Valenzuela, B. Yellampalle, M. J. Schmitt, and K.-Y. Kim, J. Opt. Soc. Am. B **25**, 1988 (2008).
[16] W. Liu, J. Bernhardt, F. Théberge, S. L. Chin, M. Châteauneuf, and J. Dubois, J. Appl. Phys. **102**, 033111 (2007).
[17] J. Bernhardt, W. Liu, F. Théberge, H. L. Xu, J. F. Daigle, M. Châteauneuf, J. Dubois, and S. L. Chin, Opt. Commun. **281**, 1268 (2008).
[18] F. Vidal, D. Comtois, C.-Y. Chien, A. Desparois, B. La Fontaine, T. W. Johnston, J.-C. Kieffer, H. P. Mercure, H. Pépin, and F. A. Rizk, IEEE Trans. Plasma Sci. **28**, 418 (2000).
[19] S. Varma, Y.-H. Chen, and H. M. Milchberg, Phys. Rev. Lett. **101**, 205001 (2008).
[20] R. W. Lewis, P. Nithiarasu, and K. N. Seetharamu, *Fundamentals of the finite element method for heat and fluid flow* (John Wiley & Sons, 2004).
[21] A. Fridman and L. A. Kennedy, *Plasma physics and engineering* (Taylor & Francis, 2004).
[22] J. D. Huba, *2009 NRL plasma formulary* (Washington, DC, 2009).
[23] C. Guo, M. Li, J. P. Nibarger, and G. N. Gibson, Phys. Rev. A **58**, R4271 (1998).
[24] J. Kasparian, R. Sauerbrey, and S. L. Chin, Appl. Phys. B **71**, 877 (2000).
[25] P. M. Mul and J. W. McGowan, J. Phys. B **12**, 1591 (1979).
[26] M. Capitelli, C. M. Ferreira, B. F. Gordiets, and A. I. Osipov, *Plasma kinetics in atmospheric gases* (Springer, 2000).
[27] G. D. Billing and E. R. Fisher, Chem. Phys. **43**, 395 (1979).
[28] I. E. Zabelinskii, O. E. Krivonosova, and O. P. Shatalov, Sov. J. Chem. Phys. **4**, 42 (1985).
[29] B. Wolf, *Handbook of ion sources* (CRC Press, 1995)
.